Frontiers of Physics
https://doi.org/10.1007/s11467-021-1109-2
Front. Phys.
17(2), 23203 (2022)

TOPICAL REVIEW

Structure search of two-dimensional systems using CALYPSO methodology

Pengyue Gao[1,2], Bo Gao[3], Shaohua Lu[4], Hanyu Liu[1,2], Jian Lv[1,2,†], Yanchao Wang[1,2], Yanming Ma[1,2,5]

[1] *International Center for Computational Method & Software, College of Physics, Jilin University, Changchun 130012, China*
[2] *State Key Laboratory of Superhard Materials, College of Physics, Jilin University, Changchun 130012, China*
[3] *Center for Green Research on Energy and Environmental Materials (GREEN) and International Center for Materials Nanoarchitectonics (MANA), National Institute for Materials Science, 1-1 Namiki, Tsukuba, Ibaraki 305-0044, Japan*
[4] *College of Materials Science and Engineering, Zhejiang University of Technology, Hangzhou 310014, China*
[5] *International Center of Future Science, Jilin University, Changchun 130012, China*
Corresponding author. E-mail: [†] *lvjian@jlu.edu.cn*
Received April 26, 2021; accepted July 14, 2021

The dimensionality of structures allows materials to be classified into zero-, one-, two-, and three-dimensional systems. Two-dimensional (2D) systems have attracted a great deal of attention and typically include surfaces, interfaces, and layered materials. Due to their varied properties, 2D systems hold promise for applications such as electronics, optoelectronics, magnetronics, and valleytronics. The design of 2D systems is an area of intensive research because of the rapid development of *ab initio* structure-searching methods. In this paper, we highlight recent research progress on accelerating the design of 2D systems using the CALYPSO methodology. Challenges and perspectives for future developments in 2D structure prediction methods are also presented.

Keywords two-dimensional (2D) systems, CALYPSO, structure prediction

Contents

1 Introduction

Reduced dimensionality is a versatile approach for discovering exotic materials, whose physical properties are entirely different from those of their bulk form. Two-dimensional (2D) systems, including 2D layered materials, surfaces, and interfaces, have attracted much attention over recent decades due to their desirable properties. Graphene is the first "modern" 2D material, first isolated in 2004 [1]. It has high carrier mobility [2, 3] and a room-temperature quantum Hall effect [4, 5], making it suitable for use in nanoelectronics and as a saturable absorber [6]. Other examples include hydrogen-terminated diamond surfaces, which are promising materials for field-effect transistor devices due to their generated 2D-hole gases [7], and the heterojunction interface between $SrTiO_3$ and $LaAlO_3$, which allows the rare coexistence of superconductivity and ferromagnetism [8, 9].

The atomic-level structure of a material plays a key role in the physical and chemical properties of 2D systems, so determination of their structures is central to the design and exploration of new 2D systems. Structure prediction relies on locating the global free-energy minimum of the potential energy surface (PES), defined as the function of the energy of a structure and its atomic coordination. Therefore, structure prediction can be mathematically formulated as a global optimization problem of the PES. Due to the exponential growth of local minima (metastable phases) with increasing numbers of atoms in a system, the number of possible metastable phases of the PES is astronomically large [10], so exhaustive ergodic search strategies are impossible, even for systems with only several atoms per unit cell. There therefore needs to develop efficient and smart computational approaches, particularly for 2D structure prediction, to quickly locate the globally stable structure in the vast structural space of the PES.

Various global optimization algorithms have been reported for structure predictions based on chemical composition by reducing the search space or enhancing the sampling efficiency of PES. These algorithms have aided

* This article can also be found at http://journal.hep.com.cn/fop/EN/10.1007/s11467-021-1109-2.

© Higher Education Press 2022

the development of structure prediction methods and include simulated annealing [11], minima hopping [12], basin hopping [13], metadynamics [14], random sampling [15], the genetic algorithm (GA) [10, 16–20], and the particle-swarm optimization (PSO) algorithm [21–23]. Some of these methods have been used to search structures of 2D systems. For example, Chen *et al.* explored 2D ice structures using random sampling methods [24], Tikhomirova *et al.* proposed a hexagonal NaCl thin film based on the GA algorithm [25], and Zhu *et al.* identified the 2D structures of tellurium using the PSO algorithm [26].

The CALYPSO (Crystal structure AnaLYsis by Particle Swarm Optimization) method [22, 23] is a highly efficient numerical method for crystal structure searches based only on chemical compositional information. The method comprises several modules dealing with structure, such as structure generation with constraints of symmetry, structure characterization using a bond characterization matrix, and structure evolution using the swarm-intelligence algorithm. The CALYPSO method has been widely used to design and discover 2D systems, including 2D materials [27–29], surfaces [30] and interfaces [31]. Attractive features have been implemented in CALYPSO to resolve various structure prediction problems, including 3D solids [22, 23], 0D nanoclusters or molecules [32], solid–solid transition states [33], X-ray diffraction data-assisted structure searches [34], and the inverse design of novel functional materials (e.g., superhard, electride, and optical materials) [35, 36]. The details of CALYPSO methodology and its applications can be found in Ref [37–39].

To date, CALYPSO has been extensively used to design materials in 2D systems and many 2D materials with interesting properties have been discovered [40]. In this work, we focus on applications of CALYPSO methodology to structure searches of 2D systems, discussing 2D layered materials in Section 2, surface construction in Section 3, and solid–solid interfaces in Section 4.

2 Two-dimensional layered materials

Nowadays, CALYPSO methodology is able to design of various 2D materials, including predicting the structures of single layer, multi-layer, thin-film 2D materials and atomic adsorption on these materials. The slab model was adopted in the CALYPSO method and involves vacuum and layered atomic structures.

(i) For single-layer materials, the random atomic positions of 2D layered structures are achieved under the constraints of 2D planar symmetry. Meanwhile, a distortion perpendicular to the in-plane layer is allowed to predict the structures of buckled layers [Fig. 1(a)].

(ii) For multi-layer materials, a van der Waals gap parameter is used to separate two adjacent layers to build the models of multilayered 2D systems [Fig. 1(b)].

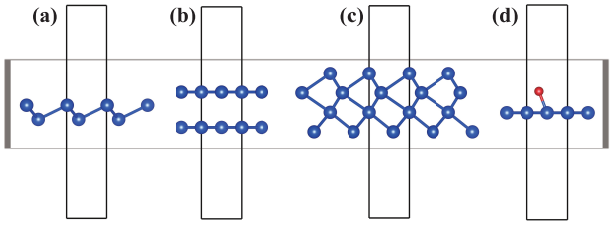

Fig. 1 The models used in CALYPSO for predicting single **(a)**, multi-layer **(b)**, film **(c)** and atomic adsorption **(d)** structures.

(iii) For thin-film systems, the atomic structure is generated by 3D symmetry constraints within a given thickness [Fig. 1(c)].

(iv) For atoms adsorbed on 2D-layered materials, the structural model involves the adsorption region on either one or both sides of a given 2D substrate [Fig. 1(d)].

The PSO algorithm in the 2D structure search models of CALYPSO [27, 28] is constrained in 2D space to evolve the generated structures.

The CALYPSO method has been widely applied in predicting various 2D materials with exotic structures and properties. Here, we focus on partial applications of the CALYPSO method to different types of 2D materials such as borophene [42, 169, 170], boron-based superconductors, hypercoordinate compounds, $ReWCl_6$, Si thin-films, and hydrogenated/oxidized graphene.

Borophenes. Since the discovery of graphene, boron, adjacent to carbon on the periodic table, has been the subject of significant effort to discover its 2D sheet structures. Boron possesses three valence electrons distributed in four available orbitals, providing a notably different bonding character to that of carbon. Diversified 2D borophenes [42, 169, 170] with triangular and hexagonal units or pure hexagonal motifs are predicted by the CALYPSO structure prediction method, and several have been synthesized [171]. Boron-based compounds such as B-C [28], B-P [117, 172], Fe-B [50], and Ti-B [71] with desirable properties have also been investigated using the CALYPSO method and will aid the design of other 2D compounds.

2D boron-based superconductors. 2D boron-based compounds have been widely explored as promising superconductors using the CALYPSO structure search method. Qu *et al.* identified the *t*-MnB_3 and *h*-MnB_3 superconductors and showed that *h*-MnB_3 has a maximum superconducting transition temperature (T_c) of 34 K at 2% tensile strain [66]. Tao *et al.* identified several orthorhombic and hexagonal MB_6 compounds (M = Mg, Ca, Ti, Y) [58] and showed that the T_c of hexagonal GaB_6 is 22.6–28.4 K under a compressive strain of 3%. Dong *et al.* predicted δ-BS and B_2C sheets with T_c values of about 21.56 K [59] and 21.20 K [59], respectively. Other 2D boron-based superconductors, such as B_2O [62, 63], XB_6 (X = Ga, In) [64],

Table 1 Novel 2D layered materials with interesting properties discovered using the CALYPSO method.

Properties	2D materials	Refs.
Topology	C, B, SiC_3, FeB_2, Be_3C_2, M_3C_2, OsC_{16}, Mg_3X_2, NiB_6, MoS_2, B_2C, $PtSe_2$, MX_2	[41–55]
Superconductivity	Mo_2B_2, YS, B_2O, W_2B_2, XB_6, $NiTe_2$, MnB_3, BS, MB_6, B_2C, CoSb	[56–67]
Hypercoordinate	Be_2C, Cu_2Si, FeB_6, TiB_4, CaSi, Zn_3O_2, Be_5C_2, TMC, o-FeC, FeB_3	[68–77]
Electronic conductivity (Li–Na ion batteries)	TaC_2, ψ-Graphene, TiC_3, TiC, P_3C, C_4N_4, MoC_2, ScC_2, ScN_2, NiC_3, B_3S, Zr_2B_2, Mo_2B_2, V_2C_2, V_2N_2, YS_2, Net-C18, t-FeC, M-graphene, C_3N, C_{5678}	[76, 78–95]
High carrier mobility	PdS_2, BeN_2, CP, Au_6S_2, BeC, BP_3, Be_2N_6, PN, MO, Cu_2S, BeN_3, AuMX_2, Cd_2C, MN_2, Au_2S, AuS, MoX_2, InP_3, PtP_2H_2, BCN, SiBCN, A_2B, PC_6N, Ga_2O_2, HfN_2, Sn_xP_y, ScN	[96–121]
(Multi) Ferromagnetism	V_3X_8, VBr_3, $FeBr_3$, $NiBr_3$, $PdBr_3$, Ge_xP_y, $CrAs_2$, Mn_2C, CrN, Co_2S_2, $CrWI_6$, $CrWGe_2Te_6$, MH_2, CoB_6, FeAs, CaCl, VSeTe, VSSe, Fe_3P, MnX,Mg_3C_2, Ti_3O_5, CrN, CuCl, $ReWCl_6$, BP_5	[122–144]
Negative Poisson ratio	Be_5C_2, SiO_2, Zn_2C, CO_2, MB_2, B_4N, SiO	[145–151]
Photocatalysts/Photovoltaics	Si, BC_3, B_4C_3, C_3H, Si-C, NP, AsP, P_4O_4, B-N-C, ψ-phosphorene, BC_2P, BC_3P_3, SiC_7, C-N	[152–165]
Half metallicity	Si_xP_y, MoN_2, MnNF	[166–168]

W_2B_2 [61] and Mo_2B_2 [57] compounds, with T_c values of <20 K, have also been designed using the CALYPSO method. Except for boron-based compositions, many superconductors with high T_c values (shown in Table 1) based on other elements have been proposed using the CALYPSO method.

Hypercoordinate materials. Chemical bonding is fundamental to compound formation. The design of materials with rule-breaking chemical bonding is desirable because of their possible unique properties. CALYPSO has been widely used to design new materials with unique chemical bonds. Li *et al.* designed a quasi-planar BeC_2 monolayer with hypercoordinate C atoms, in which each C atom binds to six Be atoms [68]. Zhang *et al.* predicted a graphene-like FeB_6 monolayer with hexa- or octa-coordinate Fe atoms [70] and found the first planar hypercoordinate transition metal in extended systems. Yang *et al.* proposed a planar Cu_2Si monolayer comprising the hexacoordinate transition metal Cu and the group IV element Si [69]. More hypercoordinate 2D materials are shown in Table 1.

$ReWCl_6$ multiferroic materials. Magnetoelectric materials are highly desirable for technological applications such as magnetocapacitors, high-performance infor-

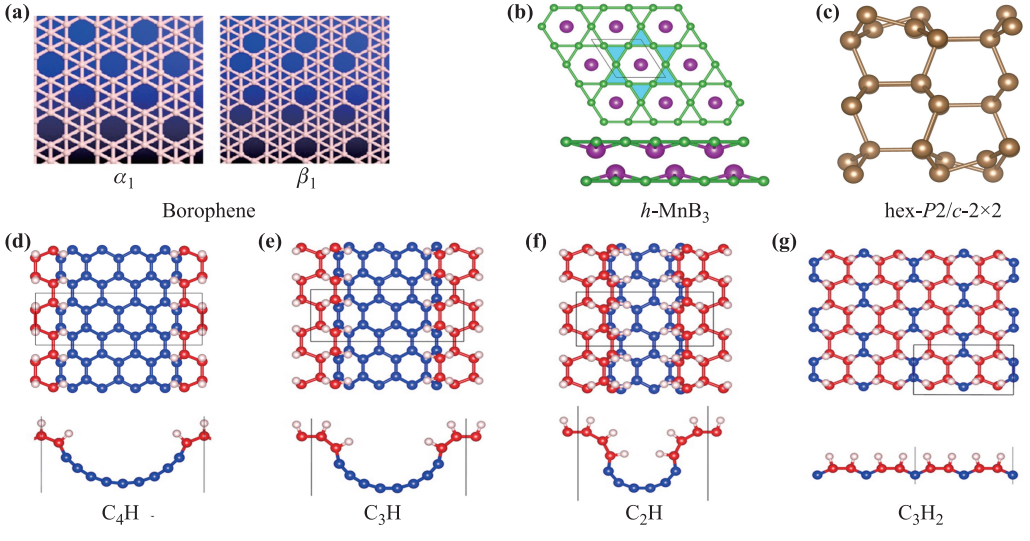

Fig. 2 The structures of **(a)** α_1-/β_1-borophene, **(b)** h-MnB_3, **(c)** hex-$P2/c$-2×2 silicene film, **(d)** C_4H, **(e)** C_3H, **(f)** C_2H, and **(g)** C_3H_2. (a) Reproduced with permission from Ref. [169], Copyright © 2012 American Chemical Society; (b) Reproduced with permission from Ref. [65], Copyright © 2020 by the American Physical Society; (d–g) Reproduced with permission from Ref [29], Copyright © 2015 American Chemical Society.

mation storage, and processing devices [173, 174]. However, there are few strong magnetoelectric materials due to the inherent exclusion between ferroelectricity and ferromagnetism. The 2D monolayer magnetoelectric material $ReWCl_6$ was proposed using the CALYPSO methodology to provide a general mechanism for understanding the electrical control of magnetism [136]. Many magnetic materials (including several multiferroic materials with coupled ferroelasticity–ferroelectricity [135, 137], or ferromagnetic–ferroelectric materials [133]) have also been designed using the CALYPSO method.

Silicene thin-film photovoltaic materials. Silicene holds promise for advanced applications in the photovoltaic industry due to its outstanding properties. Monolayer and multilayer silicenes have been synthesized on the surfaces of various metal substrates [175–182] and slices of these materials are moderately stable in air [183, 184]. However, these silicenes are unlikely to be useful as photovoltaic materials because of their metallic or semi-metallic features on metal substrates [185]. A quasi-direct gap semiconducting tri-layer silicene structure with a photovoltaic efficiency of 29% at 1.0 μm was designed using the CALYPSO method [152] and to our knowledge, exhibits the highest conversion efficiency of thin-film solar cell absorbers to date, being comparable to the conversion efficiency of bulk GaAs.

Hydrogenated/Oxidized graphene semiconductors. Graphene has attracted interest because of its exotic properties (e.g., high electronic and thermal conductivities) [186]. It has a zero band gap and is therefore not suitable for use in electronic devices, but the adsorption of H atoms efficiently opens its band gap [187]. Gao *et al.* tuned the electronic structures of graphene by adsorbing H atoms using a structure search of atomic adsorption models in the CALYPSO package [29]. Oxidized graphene has also attracted attentions [188]. The CALYPSO method predicted a novel structure of graphene monoxide [189] that is 32 meV/O energetically more stable than the previously reported mix-mode [190]. CALYPSO has also been applied to several other atom-adsorbed 2D layered materials used as electrodes: Li on B/N-doped graphene [191] and O, F, or OH on four typical MXenes: Ti_2CT_x, $Ti_3C_2T_x$, Nb_2CT_x, and $Nb_4C_3T_x$ (T = O, F, and OH) [192].

3 Surface reconstruction

The flowchart and slab model for CALYPSO surface structure search module were shown in Fig. 3. CALYPSO uses a slab model to explore surface atomic structures, in which surface structures are represented by finite slabs separated by a vacuum horizontal to the surface. Each slab has two surfaces. The bottom one is generally passivated by hydrogen atoms with integer or partial charges for covalent systems and kept unchanged for metal systems. The top

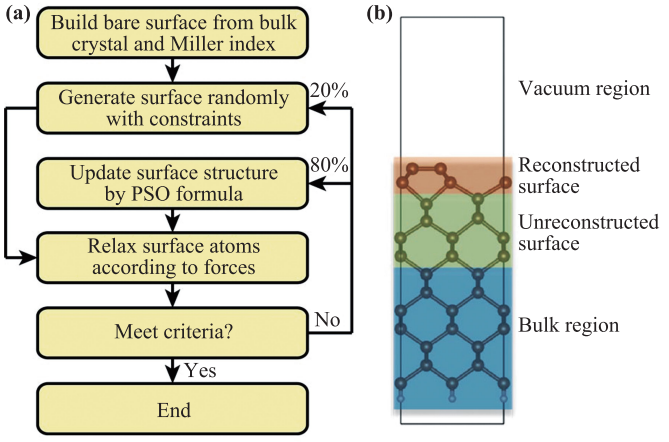

Fig. 3 **(a)** Program flowchart of the CALYPSO module for searching surface structures. **(b)** A sketch of the slab model. Reproduced with permission from Ref. [30], Copyright © 2014 Springer Nature.

surface of the slab consists of three regions, namely the bulk region with 4–8 layers, the unreconstructed surface with 2–4 layers, and the reconstructed surface. The atoms in the bulk region are fixed to keep the nature of the bulk material. And the atoms in the unreconstructed surface region are enabled to be relaxed in the process of geometric optimization. The atom positions in the reconstructed surface region are updated during the structure swarm evolution.

In the initial structural swarm-generation process, physical and chemical information, such as the plane group and electron counting rule, help to enhance surface configuration sampling efficiency. Furthermore, to improve structural diversity and ensure unbiased structure generation and coverage of the entire configuration space, a changeable number of candidate structures with lowest fitness (typically 20%) are eliminated and the same number of structures are randomly created.

Clean and chemically adsorbed diamond (100) surfaces. Diamond has both high electron and hole mobility and is one of the most promising candidates for next-generation wide-band-gap semiconductors [193]. The decreasing size of transistors results in the transistor surface playing an increasingly significant and even decisive role in determining the overall functionality of devices. Diamond films grown by techniques such as chemical vapor deposition (CVD) typically have a (100) surface, resulting in intensive theoretical and experimental studies to elucidate its properties.

Pristine diamond (100) surface. Under normal conditions, a pristine or clean diamond (100) surface has the well-known dimer surface in which the two adjacent C atoms form a symmetric dimer configuration. This structure was theoretically proposed in 1981 [194] and was obtained by resonant electron injection in 2001 [195]. The dimer surface [Fig. 4(a)] was easily located by the

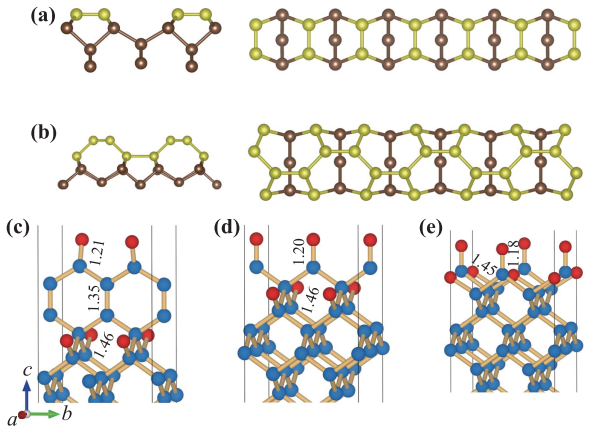

Fig. 4 The dimer **(a)** and TA1 **(b)** of the surface structures of diamond (100). Atomic structure of **(c)** ketone, **(d)** ether, and **(e)** methoxyacetone oxidized surfaces of diamond (100). Blue and red balls represent carbon and oxygen atoms, respectively. (a, b) Reproduced with permission from Ref. [30], Copyright © 2014 Springer Nature; (c–e) Reproduced with permission from Ref. [196], Copyright © 2020 Elsevier.

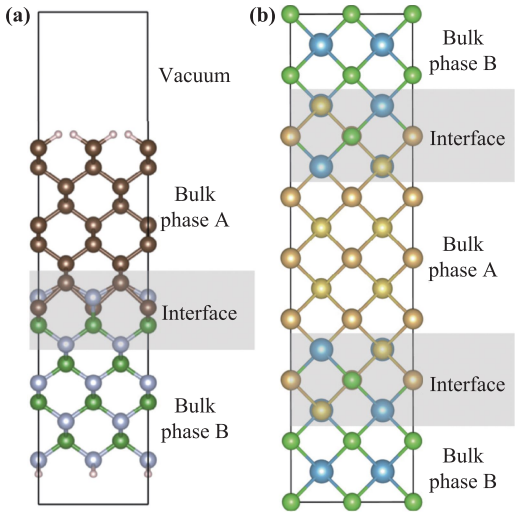

Fig. 5 Two simulated modules used in solid–solid interface structure prediction in CALYPSO. Reproduced with permission from Ref. [31], Copyright © 2019 Elsevier.

CALYPSO code as were more complicated reconstructions such as the formation of tube-like configurations. The TA1 surface [Fig. 4(b)] was energetically degenerate relative to the dimer surface under ambient conditions, but becomes energetically more favorable under compress straining or heating.

Oxygenated diamond (100) surface. Oxygenation is another commonly used technique for enhancing diamond properties. Raman and/or IR spectra show the presence of both carbonyl (C=O) and epoxide (C–O–C) moieties on oxidized diamond (100) surfaces [197, 198]. Surface structures were constructed of ketone and ether, which are fully covered by carbonyl and epoxide functional groups, respectively [199–201]. However, accurate density-functional-theory calculations indicate that the ketone surface is neither statically nor dynamically stable. The newly developed CALYPSO surface structure prediction method proposed three oxidized surfaces [Figs. 4(c)–(e)] more energetically favorable in the whole oxygen chemical-potential range [196]. The most stable surface configuration, the methoxyacetone surface, has almost no surface states in the bulk band gap, providing a perfect state for nano-sized diamond electronics.

4 Solid–solid interfaces

Solid–solid interfaces or grain boundaries (GB) are present in a broad range of materials such as heterojunctions and polycrystalline materials and often play a significant role in governing the physical properties of solids. The CALYPSO interface structure prediction method involves two main steps: (i) To reduce interfacial stress, an automatic search scheme was developed for a superlattice with minimal lattice-mismatch strain between the two bulk materials. This searched superlattice is used to create the simulated model for the subsequent interface structure search. (ii) Two simulated models have been adopted in this step. One is a slab model [Fig. 5(a)] containing a vacuum region, two bulk regions, and an interface region. The other model [Fig. 5(b)] consists of two bulk regions and two equivalent interfaces. This model effectively prevents exposure of the upper and bottom surfaces to vacuum and the influence of the dipole in a vacuum. Constraints on interatomic distance and atomic coordination number have been introduced to generate the initial interface structure to enhance search efficiency. Bulk crystal structures are fixed in the bulk region, and only the atomistic structure in the interface region is updated by a PSO algorithm designed for the interface system. Rigid-body displacement between the two bulk phases is used as a search dimension.

TiO_2 grain boundaries in photovoltaic materials. Although TiO_2 is a promising photocatalytic material, its photoreaction efficiency is limited by its large intrinsic band gap. Recently, it has been reported that introducing Ti^{3+} can improve photocatalytic efficiency [202]. The CALYPSO methodology has been used to determine the distributions of Ti^{3+} ions at the GB of the rutile $TiO_2\Sigma5(210)$ twin boundary, as shown in Figs. 6(a)–(c) [31]. The calculated results reveal that the GB can be used to engineer the electronic properties and visible-light photoactivity of TiO_2.

Interface in all-solid-state batteries. Compared to traditional Li-ion batteries, all-solid-state batteries (ASSB) have greatly improved safety and cycle stability [203, 204] due to replacement of liquid electrolyte with solid electrolyte (e.g., polymers and inorganic materials). However, high interfacial resistance between the electrode and the solid electrolyte has been reported for many ASSB

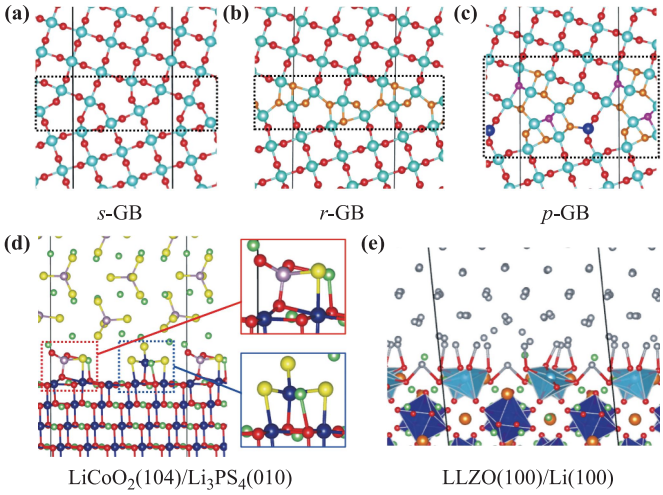

Fig. 6 Stable structures of s-GB **(a)**, r-GB **(b)**, and p-GB **(c)** of the rutile $TiO_2\Sigma5(210)$ twin boundary. The light and dark blue balls represent six- and five-coordinated Ti, respectively. The red, orange, and pink balls represent three-, four-, and five-coordinated O atoms, respectively. **(d)** The structure of the $LiCoO_2(104)/\beta$-$Li_3PS_4(010)$ interface. The green, red, blue, pink, and yellow balls represent Li, O, Co, P, and S ions, respectively. **(e)** The structure of the LLZO(100)/Li(100) interface. The orange and red spheres represent Li and O atoms, respectively. The grey and green balls represent Li atoms in Li metal and $Li_7La_3Zr_2O_{12}$ (LLZO), respectively. The light and dark blue polyhedrons indicate ZrO_5 and ZrO_6 units, respectively. (a–c) Reproduced with permission from Ref. [31], Copyright © 2019 Elsevier; (d) Reproduced with permission from Ref. [206], Copyright © 2020 American Chemical Society; (e) Reproduced with permission from Ref. [210], Copyright © 2020 American Chemical Society.

systems, limiting their practical application [205]. The microscopic origin of this interfacial resistance has been investigated using the CALYPSO interface structure prediction module to study a representative interface, the $LiCoO_2(104)$ cathode/β-$Li_3PS_4(010)$ solid electrolyte interface [206]. The predicted energetically favorable structures [Fig. 6(d)] indicate the formation of an interface reaction layer with both Co ↔ P and O ↔ S ion mixing. Calculation of the site-dependent Li chemical potentials indicate several interfacial Li sites with high Li chemical potential, resulting in the dynamical Li-depleted layer in the initial stage of charging, as determined from the calculated Li migration barriers across the interface. The calculated densities of states show the presence of interfacial electronic states, thus enhancing Li depletion at the interface. This study provides comprehensive insights into the microscopic mechanisms of interfacial Li^+ transport and resistance in ASSBs.

$Li_7La_3Zr_2O_{12}$ (LLZO) is another important solid electrolyte due to its high Li conductivity and compatibility with a Li metal anode, resulting in significant research on the LLZO/Li interface. However, several studies have reported that the LLZO/Li interface is unstable [207–209], and an in-depth understanding of instability issues is lacking, limiting further optimization of the LLZO/Li battery. The CALYPSO interface structure prediction module has been used to investigate the stability of the LLZO/Li interface [210]. Extensive sampling of the terminations of low-index (100), (001), (110), and (101) surfaces of the LLZO showed wide distribution of coordinatively unsaturated Zr (coordination number <6) sites on the surface. The energetically stable surface terminations of LLZO and Li metal were used to search the interface configurations [Fig. 6(e)]. The results indicate that the interfacial adhesion energies are dependent on surface terminations, suggesting inhomogeneous contact between LLZO and Li, which may contribute to Li dendrite growth. Undercoordinated Zr at the interfaces results in partial occupation of the Zr-4*d* conduction band, remarkably reducing LLZO. This study thus provides a theoretical explanation of the instability issues of the LLZO/Li interface.

5 Conclusion

CALYPSO methodology has been applied to structure searches of 2D systems, including 2D layered materials and atomic adsorption on these layers, surface construction, and solid–solid interfaces, and has identified several novel 2D materials with unique electrical, magnetic, or optical properties.

Despite substantial progress on 2D structure prediction of systems comprising tens of atoms, larger systems remain challenging for the current algorithm. One of the main obstacles is the computational cost of energy calculations for large systems using the first-principles method. Machine learning is a promising solution to address this as its accuracy can reach the same order of magnitude as that of the first-principles method with much lower computational cost. An accelerated CALYPSO structure prediction method based on machine learning potential has recently been developed for structure searches of large cluster systems [211]. The method reduces computational cost by one to two orders of magnitude, and the structure search is fully consistent with first-principles calculations. Other challenges, such as structure prediction at finite temperature, will be addressed in future iterations of the CALYPSO structure prediction method.

Acknowledgements This work was supported by the National Natural Science Foundation of China (Grant Nos. 12034009, 91961204, 11874175, 11874176, 11974134, and 12074138), the Strategic Priority Research Program of Chinese Academy of Sciences (Grant No. XDB33000000), the Fundamental Research Funds for the Central Universities (Jilin University, JLU), the Program for JLU Science and Technology Innovative Research Team (JLUSTIRT), and Jilin Province Outstanding Young Talents Project No. 20190103040JH.

References

1. K. S. Novoselov, Electric field effect in atomically thin carbon films, *Science* 306(5696), 666 (2004)
2. A. H. Castro Neto, F. Guinea, N. M. R. Peres, K. S. Novoselov, and A. K. Geim, The electronic properties of graphene, *Rev. Mod. Phys.* 81(1), 109 (2009)
3. J. Wang, S. Deng, Z. Liu, and Z. Liu, The rare two-dimensional materials with Dirac cones, *Natl. Sci. Rev.* 2(1), 22 (2015)
4. K. S. Novoselov, A. K. Geim, S. V. Morozov, D. Jiang, M. I. Katsnelson, I. V. Grigorieva, S. V. Dubonos, and A. A. Firsov, Two-dimensional gas of massless Dirac fermions in graphene, *Nature* 438(7065), 197 (2005)
5. Y. Zhang, Y. W. Tan, H. L. Stormer, and P. Kim, Experimental observation of the quantum Hall effect and Berry's phase in graphene, *Nature* 438(7065), 201 (2005)
6. Z. T. Wang, Y. Chen, C. J. Zhao, H. Zhang, and S. C. Wen, Switchable dual-wavelength synchronously Q-switched erbium-doped fiber laser based on graphene saturable absorber, *IEEE Photonics J.* 4(3), 869 (2012)
7. F. Maier, M. Riedel, B. Mantel, J. Ristein, and L. Ley, Origin of surface conductivity in diamond, *Phys. Rev. Lett.* 85(16), 3472 (2000)
8. A. Ohtomo and H. Y. Hwang, A high-mobility electron gas at the $LaAlO_3/SrTiO_3$ heterointerface, *Nature* 427(6973), 423 (2004)
9. J. P. Buban, Grain boundary strengthening in alumina by rare earth impurities, *Science* 311(5758), 212 (2006)
10. A. R. Oganov, and C. W. Glass, Crystal structure prediction using ab initio evolutionary techniques: Principles and applications, *J. Chem. Phys.* 124(24), 244704 (2006)
11. S. Kirkpatrick, C. D. Gelatt, and M. P. Vecchi, Optimization by simulated annealing, *Science* 220(4598), 671 (1983)
12. S. Goedecker, Minima hopping: An efficient search method for the global minimum of the potential energy surface of complex molecular systems, *J. Chem. Phys.* 120(21), 9911 (2004)
13. D. J. Wales and J. P. K. Doye, Global optimization by basin-hopping and the lowest energy structures of Lennard–Jones clusters containing up to 110 atoms, *J. Phys. Chem. A* 101(28), 5111 (1997)
14. R. Martoňák, A. Laio, and M. Parrinello, Predicting crystal structures: The Parrinello–Rahman method revisited, *Phys. Rev. Lett.* 90(7), 075503 (2003)
15. C. J. Pickard and R. J. Needs, *Ab initio* random structure searching, *J. Phys.: Condens. Matter* 23(5), 053201 (2011)
16. D. C. Lonie and E. Zurek, XtalOpt: An open-source evolutionary algorithm for crystal structure prediction, *Comput. Phys. Commun.* 182(2), 372 (2011)
17. A. N. Kolmogorov, S. Shah, E. R. Margine, A. F. Bialon, T. Hammerschmidt, and R. Drautz, New superconducting and semiconducting Fe–B compounds predicted with an *ab initio* evolutionary search, *Phys. Rev. Lett.* 105(21), 217003 (2010)
18. G. Trimarchi and A. Zunger, Global space-group optimization problem: Finding the stablest crystal structure without constraints, *Phys. Rev. B* 75(10), 104113 (2007)
19. S. Bahmann and J. Kortus, EVO — Evolutionary algorithm for crystal structure prediction, *Comput. Phys. Commun.* 184(6), 1618 (2013)
20. W. Bi, Y. Meng, R. S. Kumar, A. L. Cornelius, W. W. Tipton, R. G. Hennig, Y. Zhang, C. Chen, and J. S. Schilling, Pressure-induced structural transitions in europium to 92 GPa, *Phys. Rev. B* 83(10), 104106 (2011)
21. S. T. Call, D. Y. Zubarev, and A. I. Boldyrev, Global minimum structure searches via particle swarm optimization, *J. Comput. Chem.* 28(7), 1177 (2007)
22. Y. Wang, J. Lv, L. Zhu, and Y. Ma, CALYPSO: A method for crystal structure prediction, *Comput. Phys. Commun.* 183(10), 2063 (2012)
23. Y. Wang, J. Lv, L. Zhu, and Y. Ma, Crystal structure prediction via particle-swarm optimization, *Phys. Rev. B* 82(9), 094116 (2010)
24. J. Chen, G. Schusteritsch, C. J. Pickard, C. G. Salzmann, and A. Michaelides, Two dimensional ice from first principles: Structures and phase transitions, *Phys. Rev. Lett.* 116(2), 025501 (2016)
25. K. A. Tikhomirova, C. Tantardini, E. V. Sukhanova, Z. I. Popov, S. A. Evlashin, M. A. Tarkhov, V. L. Zhdanov, A. A. Dudin, A. R. Oganov, D. G. Kvashnin, and A. G. Kvashnin, Exotic two-dimensional structure: The first case of hexagonal NaCl, *J. Phys. Chem. Lett.* 11(10), 3821 (2020)
26. Z. Zhu, X. Cai, S. Yi, J. Chen, Y. Dai, C. Niu, Z. Guo, M. Xie, F. Liu, J. H. Cho, Y. Jia, and Z. Zhang, Multivalency-driven formation of Te-based monolayer materials: A combined first-principles and experimental study, *Phys. Rev. Lett.* 119(10), 106101 (2017)
27. Y. Wang, M. Miao, J. Lv, L. Zhu, K. Yin, H. Liu, and Y. Ma, An effective structure prediction method for layered materials based on 2D particle swarm optimization algorithm, *J. Chem. Phys.* 137(22), 224108 (2012)
28. X. Luo, J. Yang, H. Liu, X. Wu, Y. Wang, Y. Ma, S. H. Wei, X. Gong, and H. Xiang, Predicting two-dimensional boron-carbon compounds by the global optimization method, *J. Am. Chem. Soc.* 133(40), 16285 (2011)
29. B. Gao, X. Shao, J. Lv, Y. Wang, and Y. Ma, Structure prediction of atoms adsorbed on two-dimensional layer materials: Method and applications, *J. Phys. Chem. C* 119(34), 20111 (2015)
30. S. Lu, Y. Wang, H. Liu, M. S. Miao, and Y. Ma, Self-assembled ultrathin nanotubes on diamond (100) surface, *Nat. Commun.* 5(1), 3666 (2014)
31. B. Gao, P. Gao, S. Lu, J. Lv, Y. Wang, and Y. Ma, Interface structure prediction via CALYPSO method, *Sci. Bull. (Beijing)* 64(5), 301 (2019)
32. J. Lv, Y. Wang, L. Zhu, and Y. Ma, Particle-swarm structure prediction on clusters, *J. Chem. Phys.* 137(8), 084104 (2012)

33. K. Yin, P. Gao, X. Shao, B. Gao, H. Liu, J. Lv, J. S. Tse, Y. Wang, and Y. Ma, An automated predictor for identifying transition states in solids, *npj Comput. Mater.* 6(1), 16 (2020)
34. P. Gao, Q. Tong, J. Lv, Y. Wang, and Y. Ma, X-ray diffraction data-assisted structure searches, *Comput. Phys. Commun.* 213, 40 (2017)
35. Y. Zhang, H. Wang, Y. Wang, L. Zhang, and Y. Ma, Computer-assisted inverse design of inorganic electrides, *Phys. Rev. X* 7(1), 011017 (2017)
36. X. Zhang, Y. Wang, J. Lv, C. Zhu, Q. Li, M. Zhang, Q. Li, and Y. Ma, First-principles structural design of superhard materials, *J. Chem. Phys.* 138(11), 114101 (2013)
37. H. Wang, Y. Wang, J. Lv, Q. Li, L. Zhang, and Y. Ma, CALYPSO structure prediction method and its wide application, *Comput. Mater. Sci.* 112, 406 (2016)
38. Y. Wang, J. Lv, L. Zhu, S. Lu, K. Yin, Q. Li, H. Wang, L. Zhang, and Y. Ma, Materials discovery via CALYPSO methodology, *J. Phys.: Condens. Matter* 27(20), 203203 (2015)
39. Q. Tong, J. Lv, P. Gao, and Y. Wang, The CALYPSO methodology for structure prediction, *Chin. Phys. B* 28(10), 106105 (2019)
40. C. Tang, G. Kour, and A. Du, Recent progress on the prediction of two-dimensional materials using CALYPSO, *Chin. Phys. B* 28(10), 107306 (2019)
41. L. C. Xu, R. Z. Wang, M. S. Miao, X. L. Wei, Y. P. Chen, H. Yan, W. M. Lau, L. M. Liu, and Y. M. Ma, Two dimensional Dirac carbon allotropes from graphene, *Nanoscale* 6(2), 1113 (2014)
42. F. Ma, Y. Jiao, G. Gao, Y. Gu, A. Bilic, Z. Chen, and A. Du, Graphene-like two-dimensional ionic boron with double Dirac cones at ambient condition, *Nano Lett.* 16(5), 3022 (2016)
43. M. Xu, G. Zhan, S. Liu, D. Zhang, X. Zhong, Z. Qu, Y. Li, A. Du, H. Zhang, and Y. Wang, *PT*-symmetry-protected Dirac states in strain-induced hidden MoS_2 monolayer, *Phys. Rev. B* 100(23), 235435 (2019)
44. X. Tang, W. Sun, C. Lu, L. Kou, and C. Chen, Atomically thin NiB_6 monolayer: A robust Dirac material, *Phys. Chem. Chem. Phys.* 21(2), 617 (2019)
45. X. Li and Q. Wang, Prediction of a BeP_2 monolayer with a compression-induced Dirac semimetal state, *Phys. Rev. B* 97(8), 085418 (2018)
46. P. Zhou, Z. S. Ma, and L. Z. Sun, Coexistence of open and closed type nodal line topological semimetals in two dimensional B_2C, *J. Mater. Chem. C* 6(5), 1206 (2018)
47. F. Ma, G. Gao, Y. Jiao, Y. Gu, A. Bilic, H. Zhang, Z. Chen, and A. Du, Predicting a new phase (T″) of two-dimensional transition metal di-chalcogenides and strain-controlled topological phase transition, *Nanoscale* 8(9), 4969 (2016)
48. Z. H. Cui, E. Jimenez-Izal, and A. N. Alexandrova, Prediction of two-dimensional phase of boron with anisotropic electric conductivity, *J. Phys. Chem. Lett.* 8(6), 1224 (2017)
49. Y. Ding and Y. Wang, Geometric and electronic structures of two-dimensional SiC_3 compound, *J. Phys. Chem. C* 118(8), 4509 (2014)
50. H. Zhang, Y. Li, J. Hou, A. Du, and Z. Chen, Dirac state in the FeB_2 monolayer with graphene-like boron sheet, *Nano Lett.* 16(10), 6124 (2016)
51. B. Wang, S. Yuan, Y. Li, L. Shi, and J. Wang, A new Dirac cone material: A graphene-like Be_3C_2 monolayer, *Nanoscale* 9(17), 5577 (2017)
52. P. F. Liu, L. Zhou, S. Tretiak, and L. M. Wu, Two-dimensional hexagonal M_3C_2 (M = Zn, Cd and Hg) monolayers: Novel quantum spin Hall insulators and Dirac cone materials, *J. Mater. Chem. C* 5(35), 9181 (2017)
53. J. Zhou and P. Jena, Two-dimensional topological crystalline quantum spin Hall effect in transition metal intercalated compounds, *Phys. Rev. B* 95(8), 081102 (2017)
54. H. Li, Y. Xu, X. Sun, and S. Wang, Mg_3X_2 (X = C, Si) monolayer in a honeycomb-Kagome lattice: A global minimum structure, *J. Alloys Compd.* 765, 969 (2018)
55. K. Jiang, A. Cui, S. Shao, J. Feng, H. Dong, B. Chen, Y. Wang, Z. Hu, and J. Chu, New pressure stabilization structure in two-dimensional $PtSe_2$, *J. Phys. Chem. Lett.* 11(17), 7342 (2020)
56. C. Ding, G. Gong, Y. Liu, F. Zheng, Z. Zhang, H. Yang, Z. Li, Y. Xing, J. Ge, K. He, W. Li, P. Zhang, J. Wang, L. Wang, and Q. K. Xue, Signature of superconductivity in orthorhombic CoSb monolayer films on $SrTiO_3$ (001), *ACS Nano* 13(9), 10434 (2019)
57. L. Yan, T. Bo, P. F. Liu, B. T. Wang, Y. G. Xiao, and M. H. Tang, Prediction of phonon-mediated superconductivity in two-dimensional Mo_2B_2, *J. Mater. Chem. C* 7(9), 2589 (2019)
58. T. Bo, P. F. Liu, L. Yan, and B. T. Wang, Electron–phonon coupling superconductivity in two-dimensional orthorhombic MB_6 (M= Mg, Ca, Ti, Y) and hexagonal MB_6 (M= Mg, Ca, Sc, Ti), *Phys. Rev. Mater.* 4(11), 114802 (2020)
59. D. Fan, S. Lu, Y. Guo, and X. Hu, Two-dimensional stoichiometric boron carbides with unexpected chemical bonding and promising electronic properties, *J. Mater. Chem. C* 6(7), 1651 (2018)
60. Z. Qu, S. Lin, M. Xu, J. Hao, J. Shi, W. Cui, and Y. Li, Prediction of strain-induced phonon-mediated superconductivity in monolayer YS, *J. Mater. Chem. C* 7(36), 11184 (2019)
61. L. Yan, T. Bo, W. Zhang, P. F. Liu, Z. Lu, Y. G. Xiao, M. H. Tang, and B. T. Wang, Novel structures of two-dimensional tungsten boride and their superconductivity, *Phys. Chem. Chem. Phys.* 21(28), 15327 (2019)
62. H. Li, Y. Hao, D. Sun, D. Zhou, G. Liu, H. Wang, and Q. Li, Mechanical properties and superconductivity in two-dimensional B_2O under extreme strain, *Phys. Chem. Chem. Phys.* 21(46), 25859 (2019)
63. L. Yan, P. F. Liu, H. Li, Y. Tang, J. He, X. Huang, B. T. Wang, and L. Zhou, Theoretical dissection of superconductivity in two-dimensional honeycomb borophene oxide B_2O crystal with a high stability, *npj Comput. Mater.* 6(1), 94 (2020)

64. L. Yan, T. Bo, P. F. Liu, L. Zhou, J. Zhang, M. H. Tang, Y. G. Xiao, and B. T. Wang, Superconductivity in predicted two dimensional XB_6 (X = Ga, *J. Mater. Chem. C* 8(5), 1704 (2020)
65. F. Zheng, X. B. Li, P. Tan, Y. Lin, L. Xiong, X. Chen, and J. Feng, Emergent superconductivity in two-dimensional $NiTe_2$ crystals, *Phys. Rev. B* 101(10), 100505 (2020)
66. Z. Qu, F. Han, T. Yu, M. Xu, Y. Li, and G. Yang, Boron Kagome-layer induced intrinsic superconductivity in a MnB_3 monolayer with a high critical temperature, *Phys. Rev. B* 102(7), 075431 (2020)
67. D. Fan, S. Lu, C. Chen, M. Jiang, X. Li, and X. Hu, Versatile two-dimensional boron monosulfide polymorphs with tunable bandgaps and superconducting properties, *Appl. Phys. Lett.* 117(1), 013103 (2020)
68. Y. Li, Y. Liao, and Z. Chen, Be_2C monolayer with quasi-planar hexacoordinate carbons: A global minimum structure, *Angew. Chem.* 126(28), 7376 (2014)
69. L. M. Yang, V. Bačić, I. A. Popov, A. I. Boldyrev, T. Heine, T. Frauenheim, and E. Ganz, Two-dimensional Cu_2Si monolayer with planar hexacoordinate copper and silicon bonding, *J. Am. Chem. Soc.* 137(7), 2757 (2015)
70. H. Zhang, Y. Li, J. Hou, K. Tu, and Z. Chen, FeB_6 monolayers: The graphene-like material with hypercoordinate transition metal, *J. Am. Chem. Soc.* 138(17), 5644 (2016)
71. X. Qu, J. Yang, Y. Wang, J. Lv, Z. Chen, and Y. Ma, A two-dimensional TiB_4 monolayer exhibits planar octacoordinate Ti, *Nanoscale* 9(45), 17983 (2017)
72. Y. Wang, M. Qiao, Y. Li, and Z. Chen, A two-dimensional CaSi monolayer with quasi-planar pentacoordinate silicon, *Nanoscale Horiz.* 3(3), 327 (2018)
73. L. Meng, Y. Zhang, J. Zhang, and W. Wu, Completely flat 2D Zn_3O_2 monolayer with triangle and pentangle coordinated networks, *J. Phys.: Condens. Matter* 30(9), 095301 (2018)
74. Y. Wang, F. Li, Y. Li, and Z. Chen, Semi-metallic Be_5C_2 monolayer global minimum with quasi-planar pentacoordinate carbons and negative Poisson's ratio, *Nat. Commun.* 7(1), 11488 (2016)
75. C. Zhu, H. Lv, X. Qu, M. Zhang, J. Wang, S. Wen, Q. Li, Y. Geng, Z. Su, X. Wu, Y. Li, and Y. Ma, TMC (TM = Co, Ni, and Cu) monolayers with planar pentacoordinate carbon and their potential applications, *J. Mater. Chem. C* 7(21), 6406 (2019)
76. D. Fan, C. Chen, S. Lu, X. Li, M. Jiang, and X. Hu, Highly stable two-dimensional iron monocarbide with planar hypercoordinate moiety and superior Li-ion storage performance, *ACS Appl. Mater. Interfaces* 12(27), 30297 (2020)
77. C. Tang, K. K. Ostrikov, S. Sanvito, and A. Du, Prediction of room-temperature ferromagnetism and large perpendicular magnetic anisotropy in a planar hypercoordinate FeB_3 monolayer, *Nanoscale Horiz.* 6(1), 43 (2021)
78. T. Yu, S. Zhang, F. Li, Z. Zhao, L. Liu, H. Xu, and G. Yang, Stable and metallic two-dimensional TaC_2 as an anode material for lithium-ion battery, *J. Mater. Chem. A* 5(35), 18698 (2017)
79. S. Jana, S. Thomas, C. H. Lee, B. Jun, and S. U. Lee, B_3S monolayer: Prediction of a high-performance anode material for lithium-ion batteries, *J. Mater. Chem. A* 7(20), 12706 (2019)
80. G. Yuan, T. Bo, X. Qi, P.-F. Liu, Z. Huang, and B.-T. Wang, Monolayer Zr_2B_2: A promising two-dimensional anode material for Li-ion batteries, *Appl. Surf. Sci.* 480, 448 (2019)
81. T. Bo, P. F. Liu, J. Zhang, F. Wang, and B. T. Wang, Tetragonal and trigonal Mo_2B_2 monolayers: Two new low-dimensional materials for Li-ion and Na-ion batteries, *Phys. Chem. Chem. Phys.* 21(9), 5178 (2019)
82. Y. Y. Wu, T. Bo, J. Zhang, Z. Lu, Z. Wang, Y. Li, and B. T. Wang, Novel two-dimensional tetragonal vanadium carbides and nitrides as promising materials for Li-ion batteries, *Phys. Chem. Chem. Phys.* 21(35), 19513 (2019)
83. Y. Guo, T. Bo, Y. Wu, J. Zhang, Z. Lu, W. Li, X. Li, P. Zhang, and B. Wang, YS_2 monolayer as a high-efficient anode material for rechargeable Li-ion and Na-ion batteries, *Solid State Ionics* 345, 115187 (2020)
84. X. H. Cai, Q. Yang, S. Zheng, and M. Wang, Net-C18: A predicted two-dimensional planar carbon allotrope and potential for an anode in lithium-ion battery, *Energy Environ. Mater.* 4, 458 (2021)
85. G. Guo, R. Wang, S. Luo, B. Ming, C. Wang, M. Zhang, Y. Zhang, and H. Yan, Metallic two-dimensional C_3N allotropes with electron and ion channels for high-performance Li-ion battery anode materials, *Appl. Surf. Sci.* 518, 146254 (2020)
86. D. Li, Two-dimensional C_{5678}: A promising carbon-based high-performance lithium-ion battery anode, *Mater. Adv.* 2(1), 398 (2021)
87. C. Kou, Y. Tian, M. Zhang, E. Zurek, X. Qu, X. Wang, K. Yin, Y. Yan, L. Gao, M. Lu, and W. Yang, M-graphene: A metastable two-dimensional carbon allotrope, *2D Mater.* 7(2), (2020)
88. X. Li, Q. Wang, and P. Jena, ψ-graphene: A new metallic allotrope of planar carbon with potential applications as anode materials for lithium-ion batteries, *J. Phys. Chem. Lett.* 8(14), 3234 (2017)
89. T. Yu, Z. Zhao, L. Liu, S. Zhang, H. Xu, and G. Yang, TiC_3 monolayer with high specific capacity for sodium-ion batteries, *J. Am. Chem. Soc.* 140(18), 5962 (2018)
90. A. Byeon, M. Q. Zhao, C. E. Ren, J. Halim, S. Kota, P. Urbankowski, B. Anasori, M. W. Barsoum, and Y. Gogotsi, Two-dimensional titanium carbide MXene as a cathode material for hybrid magnesium/lithium-ion batteries, *ACS Appl. Mater. Interfaces* 9(5), 4296 (2017)
91. Z. Zhao, T. Yu, S. Zhang, H. Xu, G. Yang, and Y. Liu, Metallic P_3C monolayer as anode for sodium-ion batteries, *J. Mater. Chem. A* 7(1), 405 (2019)
92. T. Li, C. He, and W. Zhang, A novel porous C_4N_4 monolayer as a potential anchoring material for lithium–sulfur battery design, *J. Mater. Chem. A* 7(8), 4134 (2019)
93. Y. Yu, Z. Guo, Q. Peng, J. Zhou, and Z. Sun, Novel two-dimensional molybdenum carbides as high capacity anodes for lithium/sodium-ion batteries, *J. Mater. Chem. A* 7(19), 12145 (2019)

94. H. Huang, H. H. Wu, C. Chi, B. Huang, and T. Y. Zhang, *Ab initio* investigations of orthogonal ScC_2 and ScN_2 monolayers as promising anode materials for sodium-ion batteries, *J. Mater. Chem. A* 7(15), 8897 (2019)
95. C. Zhu, X. Qu, M. Zhang, J. Wang, Q. Li, Y. Geng, Y. Ma, and Z. Su, Planar NiC_3 as a reversible anode material with high storage capacity for lithium-ion and sodium-ion batteries, *J. Mater. Chem. A* 7(21), 13356 (2019)
96. Y. Wang, Y. Li, and Z. Chen, Not your familiar two dimensional transition metal disulfide: Structural and electronic properties of the PdS_2 monolayer, *J. Mater. Chem. C* 3(37), 9603 (2015)
97. C. Zhang and Q. Sun, A honeycomb BeN_2 sheet with a desirable direct band gap and high carrier mobility, *J. Phys. Chem. Lett.* 7(14), 2664 (2016)
98. X. Li, S. Zhang, C. Zhang, and Q. Wang, Stabilizing benzene-like planar N_6 rings to form a single atomic honeycomb BeN_3 sheet with high carrier mobility, *Nanoscale* 10(3), 949 (2018)
99. Q. Wu, W. W. Xu, L. Ma, J. Wang, and X. C. Zeng, Two-dimensional $AuMX_2$ (M = Al, Ga, In; X = S, Se) monolayers featuring intracrystalline aurophilic interactions with novel electronic and optical properties, *ACS Appl. Mater. Interfaces* 10(19), 16739 (2018)
100. L. B. Meng, S. Ni, Y. J. Zhang, B. Li, X. W. Zhou, and W. D. Wu, Two-dimensional zigzag-shaped Cd_2C monolayer with a desirable bandgap and high carrier mobility, *J. Mater. Chem. C* 6(34), 9175 (2018)
101. K. Zhao, X. Li, S. Wang, and Q. Wang, 2D planar penta-MN_2 (M = Pd, Pt) sheets identified through structure search, *Phys. Chem. Chem. Phys.* 21(1), 246 (2019)
102. Q. Wu, W. W. Xu, D. Lin, J. Wang, and X. C. Zeng, Two-dimensional gold sulfide monolayers with direct band gap and ultrahigh electron mobility, *J. Phys. Chem. Lett.* 10(13), 3773 (2019)
103. C. Tang, F. Ma, C. Zhang, Y. Jiao, S. K. Matta, K. Ostrikov, and A. Du, 2D boron dichalcogenides from the substitution of Mo with ionic B_2 pair in MoX_2 (X = S, Se and Te): High stability, large excitonic effect and high charge carrier mobility, *J. Mater. Chem. C* 7(6), 1651 (2019)
104. W. Yi, X. Chen, Z. Wang, Y. Ding, B. Yang, and X. Liu, A novel two-dimensional δ-InP_3 monolayer with high stability, tunable bandgap, high carrier mobility, and gas sensing of NO_2, *J. Mater. Chem. C* 7(24), 7352 (2019)
105. C. Pu, J. Yu, R. Yu, X. Tang, and D. Zhou, Hydrogenated PtP_2 monolayer: Theoretical predictions on the structure and charge carrier mobility, *J. Mater. Chem. C* 7(39), 12231 (2019)
106. H. Zhang, X. Li, X. Meng, S. Zhou, G. Yang, and X. Zhou, Isoelectronic analogues of graphene: The BCN monolayers with visible-light absorption and high carrier mobility, *J. Phys.: Condens. Matter* 31(12), 125301 (2019)
107. Y. Qian, H. Wu, E. Kan, and K. Deng, Graphene-like quaternary compound SiBCN: A new wide direct band gap semiconductor predicted by a first-principles study, *EPL* 118(1), 17002 (2017)
108. G. Wang, R. Pandey, and S. P. Karna, Carbon phosphide monolayers with superior carrier mobility, *Nanoscale* 8(16), 8819 (2016)
109. X. Chen, D. Wang, X. Liu, L. Li, and B. Sanyal, Two-dimensional square-A_2B (A = Cu, Ag, Au, and B = S, Se): Auxetic semiconductors with high carrier mobilities and unusually low lattice thermal conductivities, *J. Phys. Chem. Lett.* 11(8), 2925 (2020)
110. C. Wang, T. Yu, A. Bergara, X. Du, F. Li, and G. Yang, Anisotropic PC_6N monolayer with wide band gap and ultrahigh carrier mobility, *J. Phys. Chem. C* 124(7), 4330 (2020)
111. Y. Sun, B. Xu, and L. Yi, HfN_2 monolayer: A new direct-gap semiconductor with high and anisotropic carrier mobility, *Chin. Phys. B* 29(2), 023102 (2020)
112. Y. M. Dou, C. W. Zhang, P. Li, and P. J. Wang, Sn_xP_y monolayers: A new type of two-dimensional materials with high stability, carrier mobility, and magnetic properties, *Nanoscale Res. Lett.* 15(1), 155 (2020)
113. D. Liang, T. Jing, D. Mingsen, and S. Cai, Two-dimensional ScN with high carrier mobility and unexpected mechanical properties, *Nanotechnology* 32(15), 155201 (2021)
114. L. Shao, X. Duan, Y. Li, F. Zeng, H. Ye, and P. Ding, Two-dimensional Ga_2O_2 monolayer with tunable band gap and high hole mobility, *Phys. Chem. Chem. Phys.* 23(1), 666 (2021)
115. Q. Wu, W. W. Xu, B. Qu, L. Ma, X. Niu, J. Wang, and X. C. Zeng, Au_6S_2 monolayer sheets: Metallic and semiconducting polymorphs, *Mater. Horiz.* 4(6), 1085 (2017)
116. C. S. Liu, H. H. Zhu, X. J. Ye, and X. H. Yan, Prediction of a new BeC monolayer with perfectly planar tetracoordinate carbons, *Nanoscale* 9(18), 5854 (2017)
117. F. Shojaei and H. S. Kang, Partially Planar BP3 with High Electron Mobility as a Phosphorene Analog, *J. Mater. Chem. C* 5(43), 11267 (2017)
118. F. Li, Y. Wang, H. Wu, Z. Liu, U. Aeberhard, and Y. Li, Benzene-like N6 rings in a Be_2N_6 monolayer: A stable 2D semiconductor with high carrier mobility, *J. Mater. Chem. C* 5(44), 11515 (2017)
119. L. Zhao, W. Yi, J. Botana, F. Gu, and M. Miao, Nitrophosphorene: A 2D semiconductor with both large direct gap and superior mobility, *J. Phys. Chem. C* 121(51), 28520 (2017)
120. Y. Guo, L. Ma, K. Mao, M. Ju, Y. Bai, J. Zhao, and X. C. Zeng, Eighteen functional monolayer metal oxides: Wide bandgap semiconductors with superior oxidation resistance and ultrahigh carrier mobility, *Nanoscale Horiz.* 4(3), 592 (2019)
121. Y. Guo, Q. Wu, Y. Li, N. Lu, K. Mao, Y. Bai, J. Zhao, J. Wang, and X. C. Zeng, Copper(i) sulfide: A two-dimensional semiconductor with superior oxidation resistance and high carrier mobility, *Nanoscale Horiz.* 4(1), 223 (2019)
122. H. Xiao, X. Wang, R. Wang, L. Xu, S. Liang, and C. Yang, Intrinsic magnetism and biaxial strain tuning in two-dimensional metal halides V_3X_8 (X = F, Cl, Br, I) from first principles and Monte Carlo simulation, *Phys. Chem. Chem. Phys.* 21(22), 11731 (2019)

123. J. Sun, X. Zhong, W. Cui, J. Shi, J. Hao, M. Xu, and Y. Li, The intrinsic magnetism, quantum anomalous Hall effect and Curie temperature in 2D transition metal trihalides, *Phys. Chem. Chem. Phys.* 22(4), 2429 (2020)

124. Y. Jiao, W. Wu, F. Ma, Z. M. Yu, Y. Lu, X. L. Sheng, Y. Zhang, and S. A. Yang, Room temperature ferromagnetism and antiferromagnetism in two-dimensional iron arsenides, *Nanoscale* 11(35), 16508 (2019)

125. L. Zhang, G. Shi, B. Peng, P. Gao, L. Chen, N. Zhong, L. Mu, L. Zhang, P. Zhang, L. Gou, Y. Zhao, S. Liang, J. Jiang, Z. Zhang, H. Ren, X. Lei, R. Yi, Y. Qiu, Y. Zhang, X. Liu, M. Wu, L. Yan, C. Duan, S. Zhang, and H. Fang, Novel 2D CaCl crystals with metallicity, room-temperature ferromagnetism, heterojunction, piezoelectricity-like property, and monovalent calcium ions, *Natl. Sci. Rev.* 8(7), nwaa274 (2020)

126. Z. Guan, and S. Ni, Strain-controllable high curie temperature, large valley polarization, and magnetic crystal anisotropy in a 2D ferromagnetic Janus VSeTe monolayer, *ACS Appl. Mater. Interfaces* 12(47), 53067 (2020)

127. Z. Guan and S. Ni, Predicted 2D ferromagnetic Janus VSeTe monolayer with high curie temperature, large valley polarization and magnetic crystal anisotropy, *Nanoscale* 12(44), 22735 (2020)

128. C. Zhang, Y. Nie, S. Sanvito, and A. Du, First-principles prediction of a room-temperature ferromagnetic Janus VSSe monolayer with piezoelectricity, ferroelasticity, and large valley polarization, *Nano Lett.* 19(2), 1366 (2019)

129. S. Zheng, C. Huang, T. Yu, M. Xu, S. Zhang, H. Xu, Y. Liu, E. Kan, Y. Wang, and G. Yang, High-temperature ferromagnetism in an Fe_3P monolayer with a large magnetic anisotropy, *J. Phys. Chem. Lett.* 10(11), 2733 (2019)

130. B. Wang, Y. Zhang, L. Ma, Q. Wu, Y. Guo, X. Zhang, and J. Wang, MnX (X = P, As) monolayers: A new type of two-dimensional intrinsic room temperature ferromagnetic half-metallic material with large magnetic anisotropy, *Nanoscale* 11(10), 4204 (2019)

131. H. Pan, Y. Han, J. Li, H. Zhang, Y. Du, and N. Tang, Half-metallicity in a honeycomb–Kagome-lattice Mg_3C_2 monolayer with carrier doping, *Phys. Chem. Chem. Phys.* 20(20), 14166 (2018)

132. M. Xu, X. Zhong, J. Lv, W. Cui, J. Shi, V. Kanchana, G. Vaitheeswaran, J. Hao, Y. Wang, and Y. Li, Ti-fraction-induced electronic and magnetic transformations in titanium oxide films, *J. Chem. Phys.* 150(15), 154704 (2019)

133. W. Luo, K. Xu, and H. Xiang, Two-dimensional hyperferroelectric metals: A different route to ferromagnetic-ferroelectric multiferroics, *Phys. Rev. B* 96(23), 235415 (2017)

134. P. Li, W. Zhang, D. Li, C. Liang, and X. C. Zeng, Multifunctional binary monolayers Ge_xP_y: Tunable band gap, ferromagnetism, and photocatalyst for water splitting, *ACS Appl. Mater. Interfaces* 10(23), 19897 (2018)

135. Y. Gao, M. Wu, and X. C. Zeng, Phase transitions and ferroelasticity–multiferroicity in bulk and two-dimensional silver and copper monohalides, *Nanoscale Horiz.* 4(5), 1106 (2019)

136. M. Xu, C. Huang, Y. Li, S. Liu, X. Zhong, P. Jena, E. Kan, and Y. Wang, Electrical control of magnetic phase transition in a type-I multiferroic double-metal trihalide monolayer, *Phys. Rev. Lett.* 124(6), 067602 (2020)

137. H. Wang, X. Li, J. Sun, Z. Liu, and J. Yang, BP_5 monolayer with multiferroicity and negative Poisson's ratio: A prediction by global optimization method, *2D Mater.* 4(4), 045020 (2017)

138. B. Wang, H. Gao, Q. Lu, W. Xie, Y. Ge, Y. H. Zhao, K. Zhang, and Y. Liu, Type-I and type-II nodal lines coexistence in the antiferromagnetic monolayer $CrAs_2$, *Phys. Rev. B* 98(11), 115164 (2018)

139. L. Hu, X. Wu, and J. Yang, Mn_2C monolayer: A 2D antiferromagnetic metal with high Néel temperature and large spin–orbit coupling, *Nanoscale* 8(26), 12939 (2016)

140. S. Zhang, Y. Li, T. Zhao, and Q. Wang, Robust ferromagnetism in monolayer chromium nitride, *Sci. Rep.* 4(1), 5241 (2015)

141. Y. Zhang, J. Pang, M. Zhang, X. Gu, and L. Huang, Two-dimensional Co_2S_2 monolayer with robust ferromagnetism, *Sci. Rep.* 7(1), 15993 (2017)

142. C. Huang, J. Feng, F. Wu, D. Ahmed, B. Huang, H. Xiang, K. Deng, and E. Kan, Toward intrinsic room-temperature ferromagnetism in two-dimensional semiconductors, *J. Am. Chem. Soc.* 140(36), 11519 (2018)

143. Q. Wu, Y. Zhang, Q. Zhou, J. Wang, and X. C. Zeng, Transition-metal dihydride monolayers: A new family of two-dimensional ferromagnetic materials with intrinsic room-temperature half-metallicity, *J. Phys. Chem. Lett.* 9(15), 4260 (2018)

144. X. Tang, W. Sun, Y. Gu, C. Lu, L. Kou, and C. Chen, CoB_6 Monolayer: A robust two-dimensional ferromagnet, *Phys. Rev. B* 99(4), 045445 (2019)

145. Y. Wang, F. Li, Y. Li, and Z. Chen, Semi-metallic Be_5C_2 monolayer global minimum with quasi-planar pentacoordinate carbons and negative Poisson's ratio, *Nat. Commun.* 7(1), 11488 (2016)

146. Z. Gao, X. Dong, N. Li, and J. Ren, Novel two-dimensional silicon dioxide with in-plane negative Poisson's ratio, *Nano Lett.* 17(2), 772 (2017)

147. L. Meng, Y. Zhang, M. Zhou, J. Zhang, X. Zhou, S. Ni, and W. Wu, Unique zigzag-shaped buckling Zn_2C monolayer with strain-tunable band gap and negative Poisson ratio, *Inorg. Chem.* 57(4), 1958 (2018)

148. S. Liu, H. Du, G. Li, L. Li, X. Shi, and B. Liu, Two-dimensional carbon dioxide with high stability, a negative Poisson's ratio and a huge band gap, *Phys. Chem. Chem. Phys.* 20(31), 20615 (2018)

149. C. Zhang, T. He, S. K. Matta, T. Liao, L. Kou, Z. Chen, and A. Du, Predicting novel 2D MB_2 (M = Ti, Hf, V, Nb, Ta) monolayers with ultrafast Dirac transport channel and electron-orbital controlled negative Poisson's ratio, *J. Phys. Chem. Lett.* 10(10), 2567 (2019)

150. B. Wang, Q. Wu, Y. Zhang, L. Ma, and J. Wang, Auxetic B_4N monolayer: A promising 2D material with in-plane negative Poisson's ratio and large anisotropic mechanics, *ACS Appl. Mater. Interfaces* 11(36), 33231 (2019)

151. H. Du, G. Li, J. Chen, Z. Lv, Y. Chen, and S. Liu, A novel SiO monolayer with a negative Poisson's ratio and Dirac semimetal properties, *Phys. Chem. Chem. Phys.* 22(35), 20107 (2020)
152. J. Lv, M. Xu, S. Lin, X. Shao, X. Zhang, Y. Liu, Y. Wang, Z. Chen, and Y. Ma, Direct-gap semiconducting tri-layer silicene with 29% photovoltaic efficiency, *Nano Energy* 51(July), 489 (2018)
153. H. Zhang, Y. Liao, G. Yang, and X. Zhou, Theoretical studies on the electronic and optical properties of honeycomb BC_3 monolayer: A promising candidate for metal-free photocatalysts, *ACS Omega* 3(9), 10517 (2018)
154. H. Wang, X. Li, Z. Liu, and J. Yang, ψ-phosphorene: A new allotrope of phosphorene, *Phys. Chem. Chem. Phys.* 19(3), 2402 (2017)
155. X. Fu, J. Guo, L. Li, and T. Dai, Structural and electronic properties of predicting two-dimensional BC_2P and BC_3P_3 monolayers by the global optimization method, *Chem. Phys. Lett.* 726, 69 (2019)
156. J. Guan, L. Zhang, K. Deng, Y. Du, and E. Kan, Computational dissection of 2D SiC_7 monolayer: A direct band gap semiconductor and high power conversion efficiency, *Adv. Theory Simul.* 2(8), 1900058 (2019)
157. C. Kou, Y. Tian, L. Gao, M. Lu, M. Zhang, H. Liu, D. Zhang, X. Cui, and W. Yang, Theoretical design of two-dimensional carbon nitrides, *Nanotechnology* 31(49), 495707 (2020)
158. H. Chang, K. Tu, X. Zhang, J. Zhao, X. Zhou, and H. Zhang, B_4C_3 monolayer with impressive electronic, optical, and mechanical properties: A potential metal-free photocatalyst for CO_2 reduction under visible light, *J. Phys. Chem. C* 123(41), 25091 (2019)
159. Y. Ding, X. Nie, H. Dong, N. Rujisamphan, and Y. Li, Predicting a new graphene derivative C_3H as potential photocatalyst for water splitting and CO_2 reduction, *Physica E* 127, 114562 (2021)
160. J. Zhang, J. Ren, H. Fu, Z. Ding, H. Li, and S. Meng, Two-dimensional silicon-carbon hybrids with a honeycomb lattice: New family for two-dimensional photovoltaic materials, *Sci. China Phys. Mech. Astron.* 58(10), 106801 (2015)
161. D. Fan, S. Lu, Y. Guo, and X. Hu, Novel bonding patterns and optoelectronic properties of the two-dimensional Si_xC_y monolayers, *J. Mater. Chem. C* 5(14), 3561 (2017)
162. Y. Chen, Z. Lao, B. Sun, X. Feng, S. A. T. Redfern, H. Liu, J. Lv, H. Wang, and Z. Chen, Identifying the ground-state NP sheet through a global structure search in two-dimensional space and its promising high-efficiency photovoltaic properties, *ACS Mater. Lett.* 1(3), 375 (2019)
163. X. Cai, Y. Chen, B. Sun, J. Chen, H. Wang, Y. Ni, L. Tao, H. Wang, S. Zhu, X. Li, Y. Wang, J. Lv, X. Feng, S. A. T. Redfern, and Z. Chen, Two-dimensional blue-AsP monolayers with tunable direct band gap and ultrahigh carrier mobility show promising high-performance photovoltaic properties, *Nanoscale* 11(17), 8260 (2019)
164. W. Luo and H. Xiang, Two-dimensional phosphorus oxides as energy and information materials, *Angew. Chem. Int. Ed.* 55(30), 8575 (2016)
165. M. Zhang, G. Gao, A. Kutana, Y. Wang, X. Zou, J. S. Tse, B. I. Yakobson, H. Li, H. Liu, and Y. Ma, Two-dimensional boron–nitrogen–carbon monolayers with tunable direct band gaps, *Nanoscale* 7(28), 12023 (2015)
166. B. Huang, H. L. Zhuang, M. Yoon, B. G. Sumpter, and S. H. Wei, Highly stable two-dimensional silicon phosphides: Different stoichiometries and exotic electronic properties, *Phys. Rev. B* 91(12), 121401 (2015)
167. C. Zhang, J. Liu, H. Shen, X. Z. Li, and Q. Sun, Identifying the ground state geometry of a MoN_2 sheet through a global structure search and its tunable P-electron half-metallicity, *Chem. Mater.* 29(20), 8588 (2017)
168. Y. Hu, S. S. Li, W. X. Ji, C. W. Zhang, M. Ding, P. J. Wang, and S. S. Yan, Glide mirror plane protected nodal-loop in an anisotropic half-metallic MnNF monolayer, *J. Phys. Chem. Lett.* 11(2), 485 (2020)
169. X. Wu, J. Dai, Y. Zhao, Z. Zhuo, J. Yang, and X. C. Zeng, Two-dimensional boron monolayer sheets, *ACS Nano* 6(8), 7443 (2012)
170. X. Yu, L. Li, X. W. Xu, and C. C. Tang, Prediction of two-dimensional boron sheets by particle swarm optimization algorithm, *J. Phys. Chem. C* 116(37), 20075 (2012)
171. B. Feng, J. Zhang, Q. Zhong, W. Li, S. Li, H. Li, P. Cheng, S. Meng, L. Chen, and K. Wu, Experimental realization of two-dimensional boron sheets, *Nat. Chem.* 8(6), 563 (2016)
172. S. Liu, B. Liu, X. Shi, J. Lv, S. Niu, M. Yao, Q. Li, R. Liu, T. Cui, and B. Liu, Two-dimensional penta-BP_5 sheets: High-stability, strain-tunable electronic structure and excellent mechanical properties, *Sci. Rep.* 7(1), 2404 (2017)
173. W. Eerenstein, N. D. Mathur, and J. F. Scott, Multiferroic and magnetoelectric materials, *Nature* 442(7104), 759 (2006)
174. M. M. Vopson, Fundamentals of multiferroic materials and their possible applications, *Crit. Rev. Solid State Mater. Sci.* 40(4), 223 (2015)
175. L. Meng, Y. Wang, L. Zhang, S. Du, R. Wu, L. Li, Y. Zhang, G. Li, H. Zhou, W. A. Hofer, and H. J. Gao, Buckled silicene formation on Ir(111), *Nano Lett.* 13(2), 685 (2013)
176. B. Lalmi, H. Oughaddou, H. Enriquez, A. Kara, S. Vizzini, B. Ealet, and B. Aufray, Epitaxial growth of a silicene sheet, *Appl. Phys. Lett.* 97(22), 223109 (2010)
177. P. De Padova, P. Vogt, A. Resta, J. Avila, I. Razado-Colambo, C. Quaresima, C. Ottaviani, B. Olivieri, T. Bruhn, T. Hirahara, T. Shirai, S. Hasegawa, M. Carmen Asensio, and G. Le Lay, Evidence of Dirac fermions in multilayer silicene, *Appl. Phys. Lett.* 102(16), 163106 (2013)
178. B. Feng, Z. Ding, S. Meng, Y. Yao, X. He, P. Cheng, L. Chen, and K. Wu, Evidence of silicene in honeycomb structures of silicon on Ag(111), *Nano Lett.* 12(7), 3507 (2012)

179. A. Fleurence, R. Friedlein, T. Ozaki, H. Kawai, Y. Wang, and Y. Yamada-Takamura, Experimental evidence for epitaxial silicene on diboride thin films, *Phys. Rev. Lett.* 108(24), 245501 (2012)

180. B. Aufray, A. Kara, S. Vizzini, H. Oughaddou, C. Léandri, B. Ealet, and G. Le Lay, Graphene-like silicon nanoribbons on Ag(110): A possible formation of silicene, *Appl. Phys. Lett.* 96(18), 183102 (2010)

181. A. J. Mannix, B. Kiraly, B. L. Fisher, M. C. Hersam, and N. P. Guisinger, Silicon growth at the two-dimensional limit on Ag(111), *ACS Nano* 8(7), 7538 (2014)

182. P. De Padova, J. Avila, A. Resta, I. Razado-Colambo, C. Quaresima, C. Ottaviani, B. Olivieri, T. Bruhn, P. Vogt, M. C. Asensio, and G. Le Lay, The quasiparticle band dispersion in epitaxial multilayer silicene, *J. Phys.: Condens. Matter* 25(38), 382202 (2013)

183. P. De Padova, C. Ottaviani, C. Quaresima, B. Olivieri, P. Imperatori, E. Salomon, T. Angot, L. Quagliano, C. Romano, A. Vona, M. Muniz-Miranda, A. Generosi, B. Paci, and G. Le Lay, 24 h stability of thick multilayer silicene in air, *2D Mater.* 1(2), 021003 (2014)

184. H. Li, X. Liao, G. Chen, D. J. Hill, Z. Dong, and T. Huang, Event-triggered asynchronous intermittent communication strategy for synchronization in complex dynamical networks, *Neural Netw.* 66, 1 (2015)

185. J. Zhao, H. Liu, Z. Yu, R. Quhe, S. Zhou, Y. Wang, C. C. Liu, H. Zhong, N. Han, J. Lu, Y. Yao, and K. Wu, Rise of silicene: A competitive 2D material, *Prog. Mater. Sci.* 83, 24 (2016)

186. K. S. Novoselov, V. I. Fal ko, L. Colombo, P. R. Gellert, M. G. Schwab, and K. Kim, A roadmap for graphene., *Nature* 490(7419), 192 (2012)

187. R. Balog, B. Jørgensen, L. Nilsson, M. Andersen, E. Rienks, M. Bianchi, M. Fanetti, E. Lægsgaard, A. Baraldi, S. Lizzit, Z. Sljivancanin, F. Besenbacher, B. Hammer, T. G. Pedersen, P. Hofmann, and L. Hornekær, Bandgap opening in graphene induced by patterned hydrogen adsorption, *Nat. Mater.* 9(4), 315 (2010)

188. K. A. Mkhoyan, A. W. Contryman, J. Silcox, D. A. Stewart, G. Eda, C. Mattevi, S. Miller, and M. Chhowalla, Atomic and electronic structure of graphene-oxide, *Nano Lett.* 9(3), 1058 (2009)

189. B. Gao, X. Shao, J. Lv, Y. Wang, and Y. Ma, Structure prediction of atoms adsorbed on two-dimensional layer materials: Method and applications, *J. Phys. Chem. C* 119(34), 20111 (2015)

190. H. J. Xiang, S. H. Wei, and X. G. Gong, Structural motifs in oxidized graphene: A genetic algorithm study based on density functional theory, *Phys. Rev. B* 82(3), 035416 (2010)

191. L. Zhou, Z. F. Hou, B. Gao, and T. Frauenheim, Doped graphenes as anodes with large capacity for lithium-ion batteries, *J. Mater. Chem. A* 4(35), 13407 (2016)

192. T. Hu, M. Hu, B. Gao, W. Li, and X. Wang, Screening surface structure of MXenes by high-throughput computation and vibrational spectroscopic confirmation, *J. Phys. Chem. C* 122(32), 18501 (2018)

193. J. Isberg, High carrier mobility in single-crystal plasma-deposited diamond, *Science* 297(5587), 1670 (2002)

194. W. S. Verwoerd, A study of the dimer bond on the reconstructed (100) surfaces of diamond and silicon, *Surf. Sci.* 103(2–3), 404 (1981)

195. K. Bobrov, A. J. Mayne, and G. Dujardin, Atomic-scale imaging of insulating diamond through resonant electron injection, *Nature* 413(6856), 616 (2001)

196. S. Lu, D. Fan, C. Chen, Y. Mei, Y. Ma, and X. Hu, Ground-state structure of oxidized diamond (100) surface: An electronically nearly surface-free reconstruction, *Carbon* 159, 9 (2020)

197. T. Ando, K. Yamamoto, M. Ishii, M. Kamo, and Y. Sato, Vapour-phase oxidation of diamond surfaces in O_2 studied by diffuse reflectance Fourier-transform infrared and temperature-programmed desorption spectroscopy, *J. Chem. Soc. Faraday Trans.* 89(19), 3635 (1993)

198. P. John, N. Polwart, C. E. Troupe, and J. I. B. Wilson, The oxidation of diamond: The geometry and stretching frequency of carbonyl on the (100) surface, *J. Am. Chem. Soc.* 125(22), 6600 (2003)

199. H. Tamura, H. Zhou, K. Sugisako, Y. Yokoi, S. Takami, M. Kubo, K. Teraishi, A. Miyamoto, A. Imamura, M. N.-Gamo, and T. Ando, Periodic density-functional study on oxidation of diamond (100) surfaces., *Phys. Rev. B* 61(16), 11025 (2000)

200. S. J. Sque, R. Jones, and P. R. Briddon, Structure, electronics, and interaction of hydrogen and oxygen on diamond surfaces, *Phys. Rev. B* 73(8), 085313 (2006)

201. H. Yang, L. Xu, C. Gu, and S. B. Zhang, First-principles study of oxygenated diamond (001) surfaces with and without hydrogen, *Appl. Surf. Sci.* 253(9), 4260 (2007)

202. F. Zuo, L. Wang, T. Wu, Z. Zhang, D. Borchardt, and P. Feng, Self-doped Ti^{3+} enhanced photocatalyst for hydrogen production under visible light, *J. Am. Chem. Soc.* 132(34), 11856 (2010)

203. A. Manthiram, X. Yu, and S. Wang, Lithium battery chemistries enabled by solid-state electrolytes, *Nat. Rev. Mater.* 2(4), 16103 (2017)

204. Z. Zhang, Y. Shao, B. Lotsch, Y. S. Hu, H. Li, J. Janek, L. F. Nazar, C. W. Nan, J. Maier, M. Armand, and L. Chen, New horizons for inorganic solid state ion conductors, *Energy Environ. Sci.* 11(8), 1945 (2018)

205. K. Takada, N. Ohta, L. Zhang, K. Fukuda, I. Sakaguchi, R. Ma, M. Osada, and T. Sasaki, Interfacial modification for high-power solid-state lithium batteries, *Solid State Ion.* 179(27–32), 1333 (2008)

206. B. Gao, R. Jalem, Y. Ma, and Y. Tateyama, Li + transport mechanism at the heterogeneous cathode/solid electrolyte interface in an all-solid-state battery via the first-principles structure prediction scheme, *Chem. Mater.* 32(1), 85 (2020)

207. C. Ma, Y. Cheng, K. Yin, J. Luo, A. Sharafi, J. Sakamoto, J. Li, K. L. More, N. J. Dudney, and M. Chi, Interfacial stability of Li metal–solid electrolyte elucidated via in situ electron microscopy, *Nano Lett.* 16(11), 7030 (2016)

208. Y. Zhu, J. G. Connell, S. Tepavcevic, P. Zapol, R. Garcia-Mendez, N. J. Taylor, J. Sakamoto, B. J. Ingram, L. A. Curtiss, J. W. Freeland, D. D. Fong, and N. M. Markovic, Dopant-dependent stability of garnet solid electrolyte interfaces with lithium metal, *Adv. Energy Mater.* 9(12), 1803440 (2019)

209. F. Han, A. S. Westover, J. Yue, X. Fan, F. Wang, M. Chi, D. N. Leonard, N. J. Dudney, H. Wang, and C. Wang, High electronic conductivity as the origin of lithium dendrite formation within solid electrolytes, *Nat. Energy* 4(3), 187 (2019)

210. B. Gao, R. Jalem, and Y. Tateyama, Surface-dependent stability of the interface between garnet $Li_7La_3Zr_2O_{12}$ and the Li metal in the all-solid-state battery from first-principles calculations, *ACS Appl. Mater. Interfaces* 12(14), 16350 (2020)

211. Q. Tong, L. Xue, J. Lv, Y. Wang, and Y. Ma, Accelerating CALYPSO structure prediction by data-driven learning of a potential energy surface, *Faraday Discuss.* 211, 31 (2018)